Research Article

Diego R. Abujetas*, Nuno de Sousa, Antonio García-Martín, José M. Llorens and José A. Sánchez-Gil*

Active angular tuning and switching of Brewster quasi bound states in the continuum in magneto-optic metasurfaces

https://doi.org/10.1515/nanoph-2021-0412
Received July 28, 2021; accepted September 14, 2021; published online October 1, 2021

Abstract: Bound states in the continuum (BICs) emerge throughout physics as leaky/resonant modes that remain, however, highly localized. They have attracted much attention in photonics, and especially in metasurfaces. One of their most outstanding features is their divergent Q-factors, indeed arbitrarily large upon approaching the BIC condition (quasi-BICs). Here, we investigate how to tune quasi-BICs in magneto-optic (MO) all-dielectric metasurfaces. The impact of the applied magnetic field in the BIC parameter space is revealed for a metasurface consisting of lossless semiconductor spheres with MO response. Through our coupled electric/magnetic dipole formulation, the MO activity is found to manifest itself through the interference of the out-of-plane electric/magnetic dipole resonances with the (MO-induced) in-plane magnetic/electric dipole, leading to a rich, magnetically tuned quasi-BIC phenomenology, resembling the behavior of Brewster quasi-BICs for tilted vertical-dipole resonant metasurfaces. Such resemblance underlies our proposed design for a fast MO switch of a Brewster quasi-BIC by simply reversing the driving magnetic field. This MO-active BIC behavior is further confirmed in the optical regime for a realistic Bi:YIG nanodisk metasurface through numerical calculations. Our results present various mechanisms to magneto-optically manipulate BICs and quasi-BICs, which could be exploited throughout the electromagnetic spectrum with applications in lasing, filtering, and sensing.

Keywords: all-dielectric metasurfaces; bound states in the continuum; magneto-optics.

***Corresponding authors: Diego R. Abujetas and José A. Sánchez-Gil**, Instituto de Estructura de la Materia (IEM-CSIC), Consejo Superior de Investigaciones Científicas, Serrano 121, 28006 Madrid, Spain, E-mail: diego.romero@iem.cfmac.csic.es (D. R. Abujetas), j.sanchez@csic.es (J. A. Sánchez-Gil). https://orcid.org/0000-0002-5370-3717
Nuno de Sousa, Donostia International Physics Center (DIPC), 20018 Donostia-San Sebastián, Spain, E-mail: nunodsousa@dipc.org
Antonio García-Martín and José M. Llorens, Instituto de Micro y Nanotecnología IMN-CNM, CSIC, CEI UAM + CSIC, Isaac Newton 8, Tres Cantos, Madrid 28760, Spain, E-mail: a.garcia.martin@csic.es (A. Garca-Martn), jose.llorens@csic.es (J.M. Llorens)

1 Introduction

Lately, certain kinds of localized states that otherwise lie in the continuum of modes, called bound states in the continuum [1] (BICs), are attracting much attention, especially in photonics [2–5]. Among the various configurations exhibiting photonic BICs, metasurfaces have been widely exploited [6–9]. Such planar arrays with sub-wavelength periodicity limit the outgoing radiation channels only to the specular ones, facilitating the emergence of BICs at the Γ point from localized/leaky modes that are not allowed to radiate due to symmetry protection. A plethora of fascinating phenomenology relying on BICs, mostly stemming from their diverging Q-factors, has been explored: e.g., lasing [10–12], enhanced nonlinearities [13, 14], electromagnetically induced transparency [15], and sensing [16, 17].

Nonetheless, whereas tunable metasurfaces based on a variety of mechanisms have been proposed [18, 19], the active tunability of symmetry-protected BICs remains largely unexplored, mostly due to the strong dependence on geometrical constraints [20–28]. To the best of our knowledge, active BICs in metasurfaces have been only achieved through: photodoping a Si-based metasurface at THz [20, 21] and telecomm [22] frequencies; photosensitive chalcogenide glass metasurfaces [23]; adding a graphene layer to all-dielectric metasurfaces also at THz frequencies [24, 25]; and optomechanical control of an ad-hoc T-shaped ridge metasurface at telecomm frequencies [26]. Interestingly, magneto-optically active systems have been considered, but with the aim of using the extreme localization

of the BIC excitation to enhance the magnetic dichroism rather than using magneto-optics (MO) as a mechanism to tune BICs [24, 29, 30].

MO activity is one of the most studied effects to control the flow of light using external sources. The application of an external magnetic field induces couplings between the induced dipoles in a system with ultrafast switching times [31–35]. This allows rapid modulation of the optical properties of the materials at hand, paving the way to the development of high-performance devices such as highly sensitive sensing platforms [36–38] or to new concepts such as tunable radiative heat transfer [39, 40].

Herewith, with the aim of providing means to actively and externally control BIC emergence, we show how a canonical BIC can be tuned as a quasi-BIC through MO activity. In particular, we focus on BICs in high-refractive-index, all-dielectric meta-atoms (spheres, disks o pillars) stemming from vertical electric or magnetic dipole resonances in the visible [9, 11] or GHz [7] domains. First, its tunability is proved in Section 2 for a simple configuration consisting of a square array of lossless semiconductor nanospheres with MO activity through finite-difference time-domain (FDTD) numerical simulations, demonstrating in turn that our coupled electric/magnetic dipole (CEMD) formulation [41, 42] enables one to address such MO activity in an insightful (and much faster) manner. CEMD is then used in Section 3 to reveal the peculiar role played by the MO term in the lattice-induced dressed polarizabilities, similar to that of meta-atom tilting in the so-called Brewster quasi-BICs [7]. Thereby, means to magneto-optically switch on/off Brewster quasi-BICs by simply reversing the driving magnetic field are unveiled and explored in the near-field too in Section 4, with far-reaching implications for applications. In Section 5, the MO-BIC concept is demonstrated in a more practical configuration in the optical domain consisting of Bi:YIG nanodisk arrays, on the basis of robust BICs decoupled from the background. Finally, our concluding remarks are included in Section 6.

2 MO quasi-BICs

As a proof of principle, let us consider a square array of lossless semiconductor nanospheres, as shown in the schematic in Figure 1, with lattice constant $a = 300$ nm and sphere diameter $D = 150$ nm. Such all-dielectric metasurfaces are known to exhibit symmetry-protected magnetic-dipole (MD) BICs [41, 42], similar to those reported experimentally in the GHz [7] and visible [9, 11, 12] domains. We include a weak MO response of the semiconductor spheres in a similar way as in Ref. [43]. Upon considering an external applied magnetic field **H** oriented along the y-direction (within the plane of the sphere array and perpendicular to the plane of incidence), as shown in the schematic in Figure 1a, this results in the following tensorial permittivity:

$$\epsilon = \begin{pmatrix} \epsilon_{xx} & 0 & \epsilon_{xz}^{(\mathrm{MO})} \\ 0 & \epsilon_{yy} & 0 \\ \epsilon_{zx}^{(\mathrm{MO})} & 0 & \epsilon zz \end{pmatrix}, \tag{1}$$

where the diagonal terms are given by the usual permittivity of a semiconductor in the optical regime, assumed constant and lossless:

$$\epsilon_{xx} = \epsilon_{yy} = \epsilon_{zz} = 3.5^2, \tag{2}$$

and the MO-induced nondiagonal terms are simply assumed to be constant at this time and given by:

$$\epsilon_{xz}^{(\mathrm{MO})} = -\epsilon_{zx}^{(\mathrm{MO})} = 0.05\imath. \tag{3}$$

First, we explore the spectral dependence on the MO activity of the known BIC at the Γ point through FDTD calculations. These FDTD calculations have been performed using the commercial code Lumerical®, using periodic boundary conditions in x and y directions and perfectly matching layers in z. The discretization mesh used is 2 nm in each direction in a $200 \times 200 \times 200$ nm^3 box around the sphere, continuously growing to a maximum value of 12 nm at the boundaries, and the time span of the simulation is 2 ps. Due to the sharpness of the resonance, we need to enhance the frequency resolution of the Fourier-transformed time signal. This has been achieved with the aid of the Padé approximant [44], allowing e.g., to resolve resonances of extremely high Q-factor [45]. In the current study, we have computed the Poynting vector in the frequency domain from the time signal of the fields obtained by FDTD with the algorithm described in [46].

The resulting reflectance spectra, $R(\omega)$, for transverse-electric (TE) and transverse-magnetic (TM) linear polarizations are shown in Figure 1a, wherein the schematic depicts the scattering geometry: θ is the angle of incidence defined in the xz plane with respect to the normal to the metasurface, and the polarization angle δ is defined in such a way that the polarization vector **e** is given by

$$e_x = \cos\,\theta\,\sin\,\delta, \quad e_y = \cos\,\delta, \quad e_z = \sin\,\theta\,\sin\,\delta. \tag{4}$$

At normal incidence (Γ point) without MO activity, this semiconductor sphere metasurface is known to exhibit symmetry-protected MD and electric-dipole (ED) BICs [41, 42], which as expected are not accessible through

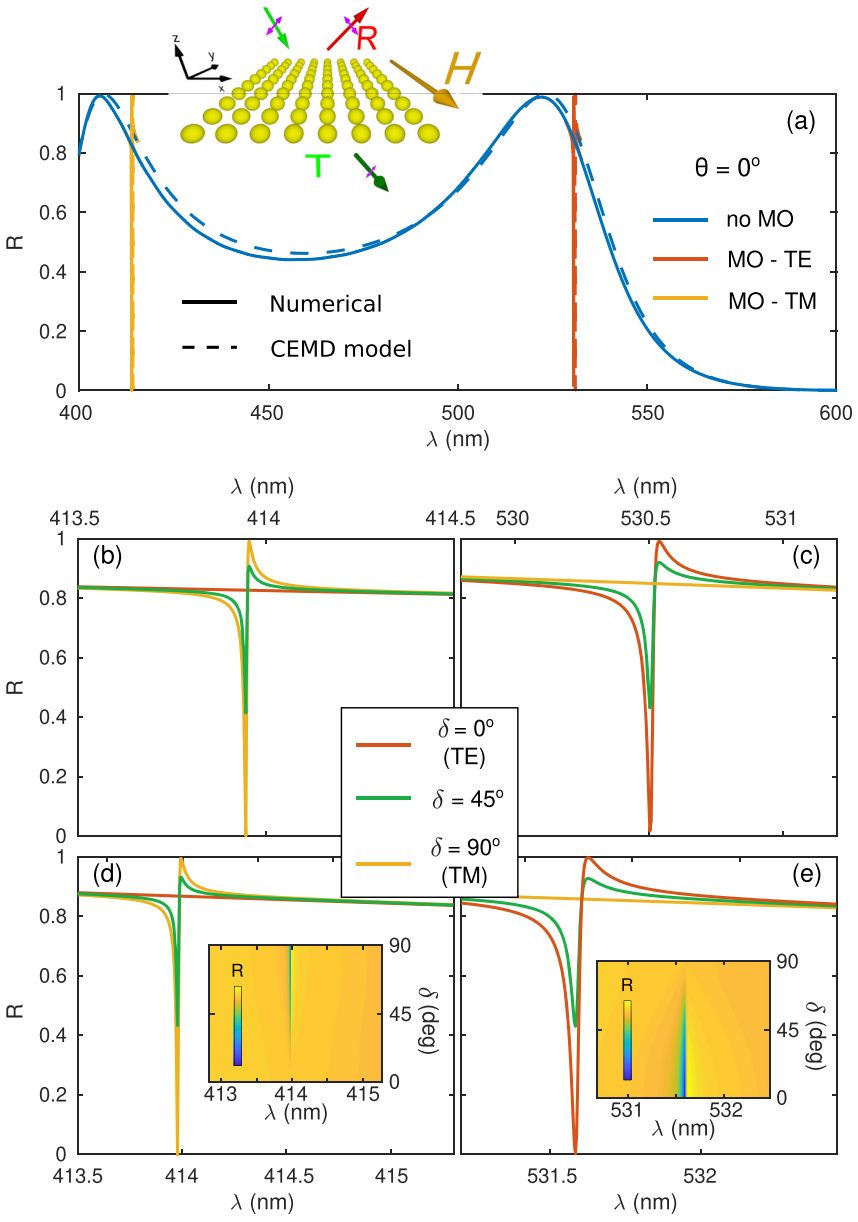

Figure 1: (a) Reflectance spectra $R(\omega)$ at normal angle of incidence $\theta = 0°$ from an infinite square array of lossless semiconductor ($n = 3.5$) nanospheres (lattice period $a = 300$ nm, sphere diameter $D = 150$ nm), as a function of the wavelength λ, calculated through FDTD simulations (solid curves) and our CEMD formulation (dashed curves), with and without MO activity, for linear polarizations: $\delta = 0°$ (TE), $\delta = 45°$, and $\delta = 90°$ (TM). MO activity is accounted for: in FDTD through a nondiagonal term in the electric permittivity, see Eqs. (1)–(3); and in CEMD through nondiagonal terms in the electric/magnetic polarizabilities, see Eq. (5). The schematic illustrates the studied metasurface configuration, indicating incident, reflected, and transmitted plane waves, along with the external magnetic field inducing the magneto-optic response. (b–e) Spectral regions around the symmetry-protected (b and d) ED-BIC and (c and e) MD-BIC are zoomed in: (b and c) FDTD; (d and e) CEMD. Insets in (d and e) show contour maps of the dependence on the entire range of linear polarization δ calculated through CEMD.

plane wave illumination at normal incidence, revealing no structure in the reflectances. Recall that the large broad backgrounds stem from the broad, lowest order MD and ED resonances of the single semiconductor spheres excited in the plane of the metasurface. The impact of the MO activity is evident in Figure 1a through the ultra-narrow bands (with diverging Q-factors) around the canonical BICs, which convert them to quasi-BICs. For TM polarization as zoomed in Figure 1b, the MO activity converts the ED-BIC at higher energies into a quasi-BIC; for TE polarization, Figure 1c, it is the MD-BIC at lower energies that emerges as a quasi-BIC. Conversely, TE/TM polarization has no impact on the ED/MD-BIC; at 45°-polarization (basically a combination of TE and TM polarizations), the MO activity affects both BICs, turning them into quasi-BICs.

Next the above-mentioned MO effects on BICs are explored analytically through our CEMD formulation for infinite planar arrays [41], which allows for much faster calculations with deeper physical insight, and in turn qualitative and quantitatively accurate as long as no higher-order multipoles are involved [7, 9, 42]. The (required) polarizabilities of the semiconductor spheres are simply given in the absence of MO activity by Mie theory, retaining only lowest-order MD and ED terms. In order to account for the MO-induced terms, we calculate numerically (COMSOL) the tensorial polarizabilities used in the CEMD formulation

depending on the MO configuration as follows: the scattering cross sections for lossless semiconductor spheres, with the tensorial permittivity used above for the FDTD calculations, are calculated with different combinations of incident field direction and polarization, and applied magnetic field direction, projecting them into the far-field in order to extract all the contributions to the tensorial polarizabilities. As expected, nondiagonal terms emerge; in our case, considering the magnetic field along the *y*-axis perpendicular to the plane of incidence (see Figure 1), this results in the following tensor polarizability:

$$\alpha^{\mathbf{E}} = \begin{pmatrix} \alpha_{xx} & 0 & \alpha_{xz}^{(\mathrm{MO})} \\ 0 & \alpha_{yy} & 0 \\ \alpha_{zx}^{(\mathrm{MO})} & 0 & \alpha_{zz} \end{pmatrix}, \tag{5}$$

with $\alpha_{xz}^{(\mathrm{MO})} = -\alpha_{xz}^{(\mathrm{MO})}$ (similarly for $\alpha^{\mathbf{H}}$).

The resulting CEMD (quasi-analytical) calculations of the reflectance spectra with/without MO activity are shown in Figure 1a, d, and e, exactly for the same configuration of semiconductor-sphere metasurface used to explore the MO-induced quasi-BICs through FDTD numerical simulations. All MO-induced features discussed above are fully confirmed, revealing indeed not only qualitative but also quantitative agreement (except for a very small frequency shift of the quasi-BIC central frequencies, mostly due to the different sphere meshes used in FDTD and in the calculation of the polarizabilities). Bear in mind that, in the FDTD numerical simulations, the MO activity is included as nondiagonal terms in the electric permittivity tensor, Eq. (1), whereas in our CEMD model such activity is accounted for through the nondiagonal terms in the electric and magnetic polarizability tensors, Eq. (5), extracted in turn from the scattering cross-sections of the semiconductor spheres with/without MO. This not only supports the accuracy of our simple CEMD formulation but also the procedure to introduce the MO activity through tensorial polarizabilities. To further illustrate the flexibility of our CEMD model, insets in Figure 1d and e show the dependence of the corresponding MO-BIC reflectance spectra on the linear polarization angle $\delta = 0° - 90°$.

3 Brewster quasi-BIC equivalence: MO tuning

We now analyze through our CEMD formulation the physics underlying the MO tuning of the quasi-BIC. Apparently, the MO activity is introducing a dipolar response at other directions away from the Γ point, inducing coupling of the vertical MD/ED (responsible for the BIC at TE/TM polarizations) into in-plane dipoles, thus breaking the symmetry protection mechanism. To shed more light on this plausible mechanism, we calculate the dependence of the MO-induced quasi-BIC on the strength of the MO term. Instead of recalculating the polarizability for different values of $\epsilon_{xz}^{(\mathrm{MO})} \propto H$ (since we are in the linear response in H), the MO-induced nondiagonal term is proportional to the previously calculated polarizability multiplied by a factor β, that will simulate the intensity of the applied magnetic field. Nonetheless, for ensuring energy conservation, instead of directly multiplying the off-diagonal term $\alpha_{xz}^{(\mathrm{MO})}$ by β (this will lead to nonconservative systems), the off-diagonal term of the inverse of the polarizability is scaled by the factor β. Specifically:

$$(1/\alpha)_{xz}^{(N)} = \beta(1/\alpha)_{xz} \propto H, \tag{6}$$

where $(1/\alpha)_{xz}$ is the off-diagonal term of the inverse of the polarizability calculated through the FDTD numerical simulations, and $(1/\alpha)_{xz}^{(N)}$ the new term of the polarizability used to model the MO effect. After that scaling, the final polarizability is obtained by inverting this new inverse polarizability, where only the off-diagonal term is modified.

The reflectance spectra for fixed (normal and off-normal) angles of incidence $\theta = 0°, 5°$ are plotted in Figure 2. At normal incidence, Figure 2a and b, the typical map of BIC spectra around the Γ point in the parameter space is evident, becoming a quasi-BIC with increasing (starting from negligible) spectral width as the parameter is tuned, with the (crucial) fact that the parameter, in this case, is the MO activity. On the other hand, we clearly observe at $\theta = 5°$ in Figure 2c and d a different scenario: a quasi-BIC exhibiting again a narrow (though finite) spectral width that becomes inaccessible at a given value in the MO parameter space of the applied magnetic field, different for each polarization.

Further confirmation of the emergence of quasi-BICs due to the MO activity is given in Figure 3, where the spectral dependence of the relevant dipole moments on each sphere is calculated at normal incidence. In the absence of magnetic activity, dipole moments show moderate, nearly constant values indicating that no resonance is excited other than the broad in-plane ones. Moreover, the out-of-plane dipole moments are not excited at normal incidence. Upon switching the magnetic field on ($\beta = 1$), the dipole moments associated with the quasi-BICs are enhanced by a few orders of magnitude: in particular, the out-of-plane electric p_z (respectively, magnetic m_z) dipole moment for TM (respectively, TE) polarization associated with the emergence of the ED quasi-BIC

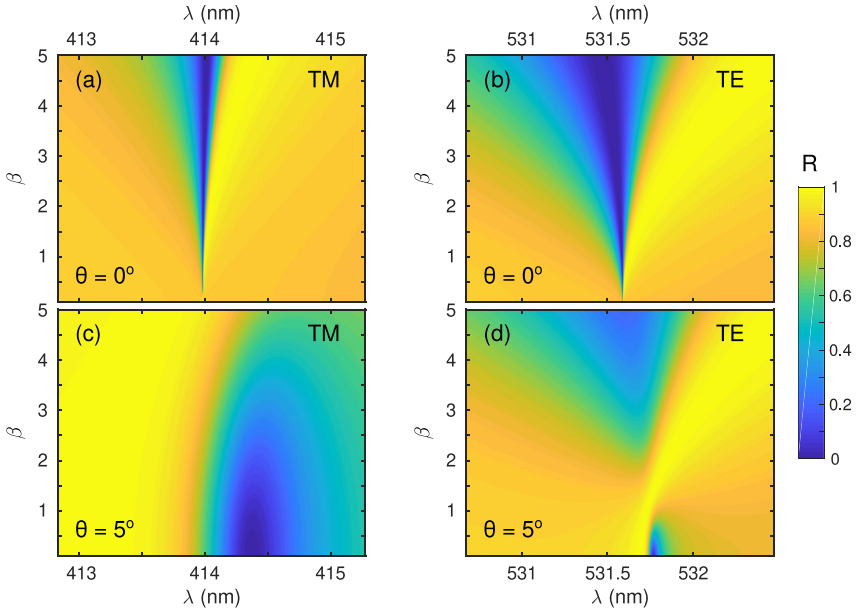

Figure 2: Contour maps of the reflectance spectra $R(\omega)$ from an infinite square array of lossless semiconductor ($n = 3.5$) nanospheres (lattice period $a = 300$ nm, sphere diameter $D = 150$ nm), at angles of incidence $\theta = 0°, 5°$, as a function of MO activity β (see text) and wavelength λ, theoretically calculated through CEMD for (a and c) TM and (b and d) TE polarizations: (a and b) normal incidence $\theta = 0°$; (c and d) non-normal angle of incidence $\theta = 5°$.

(respectively, MD quasi-BIC), see Figure 3a (respectively, b). In addition, the in-plane dipole moments oriented along the x-axis show narrow, asymmetric Fano resonances, whereas the in-plane dipole moments oriented along the y-axis (those not related with the quasi-BIC) show no change upon the application of the external magnetic field.

In essence, the impact of MO activity, as stated in our CEMD model, is formally equivalent to consider that the vertical EDs/MDs are tilted, as shown literally by tilting the disk vertical axis in high-index disk arrays in Ref. [7]. If this is so, a quasi-Brewster BIC should emerge at angles of incidence related to this effective MO-tilting. The MO activity is inducing an effective tilt to the ED (respectively, MD) resonance, proportional to the MO response for TM (respectively, TE) polarization. When the induced tilt angle equals $\theta^{\mathrm{MO}} = 5°$, as derived from the following conditions (note that the MO impact is different for each BIC, due to the different E or H polarizability terms involved):

$$\sin\theta^{(E,\mathrm{MO})} = \left|\frac{\alpha_{zx}^{(E)}}{\alpha_{zz}^{(E)}}\right|_{\omega_{\mathrm{BIC}}}, \text{TM polarization;} \tag{7}$$

$$\sin\theta^{(H,\mathrm{MO})} = \left|\frac{\alpha_{zx}^{(H)}}{\alpha_{zz}^{(H)}}\right|_{\omega_{\mathrm{BIC}}}, \text{TE polarization;} \tag{8}$$

the quasi-BIC resonant line shape disappears from the reflectance spectra in parameter space, as evidenced in Figure 2c and d. Recall that this does not mean that a BIC emerges at a different angle. As thoroughly described for tilted dipolar resonances [7], the mode is a quasi-BIC with a very large (but finite) Q-factor, which cannot either be

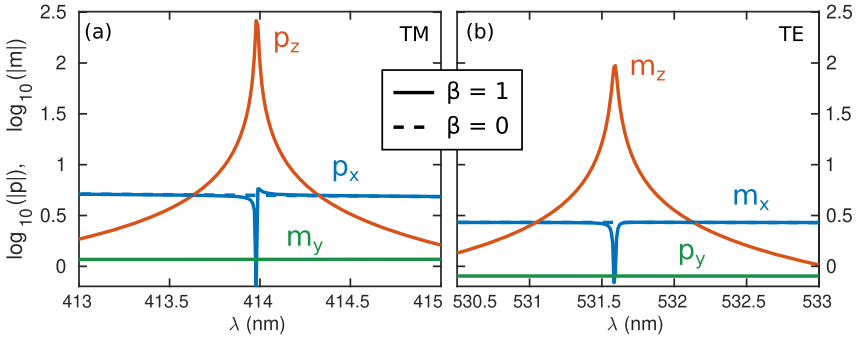

Figure 3: Spectral dependence of the relevant electric and magnetic dipolar moments (in logarithmic scale) on each sphere of an infinite square array of lossless semiconductor ($n = 3.5$) nanospheres (lattice period $a = 300$ nm, sphere diameter $D = 150$ nm) as in Figure 2a illuminated at normal incidence $\theta = 0°$, with ($\beta = 1$, solid curves), and without ($\beta = 0$, dashed curves) MO activity, theoretically calculated through CEMD in the vicinity of each BIC: (a) out-of-plane electric dipole p_z and in-plane contributions p_x, m_y for TM polarization; (b) out of plane magnetic dipole m_z and in-plane contributions m_x, p_y for TE polarization. All of them are normalized by the in-plane electric or magnetic dipole moments (p_y or m_y) that would be excited about an isolated sphere. The out-of-plane dipole moments p_z, m_z are negligible for $\beta = 0$.

excited or radiate at the tilt angle ϕ (namely, at $\theta = \pm\phi$), so-called Brewster quasi-BIC. The Q-factor is larger the closer the quasi-BIC is to the true BIC, namely, the closer is the MO activity (or the tilt angle) to zero: this explains the smaller width of the MO quasi-BIC spectra near the Brewster angle condition for TE polarization in Figure 2d, as compared to that for TM polarization in Figure 2c. It should be emphasized that, though not being a true BIC, this Brewster/MO quasi-BIC can be very useful in applications exploiting a BIC-like phenomenology (inaccessible resonances with near divergent Q-factors) at non-normal angles, such as sensing, lasing, and nonlinear processes [11, 12], with the advantage in our present configuration that the angle can be actively tuned through an applied magnetic field.

4 Brewster quasi-BIC MO switching

Next, we focus on another peculiar feature of Brewster quasi-BICs: they are not fully symmetric upon mirror-symmetric illumination with respect to the metasurface normal, that is, upon illuminating with $\pm\theta$. As discussed in Ref. [7], when the angle of incidence is aligned with the tilted disk axis, no resonance is excited and light traverses the metasurface unaltered. By contrast, when the angle of incidence is minus that tilt angle, the resonance (quasi-BIC) is excited, nonetheless leading to no reflection and full transmission (by reciprocity) through the interference of the quasi-BIC scattered field with the incident field. Let us explore this phenomenology in the case of MO activity, addressing in turn the near-field footprint (not done in Ref. [7]). To this end, we investigate near-field maps calculated through our CEMD model [42] at spectral/angular regions close to the MO quasi-BIC wavelength and incident angle (equivalent to the Brewster quasi-BIC tilt angle) observed in the far-field spectra in Figure 2. Moreover, we take advantage of the equivalence between the applied magnetic field direction and the sign of the resulting Brewster quasi-BIC tilt angle, to explore MO tunability with varying angle of incidence, so that reversing the magnetic field direction (π rotation) is formally identical to changing the sign of the angle of incidence.

First, we make evident the asymmetry in the far-field mentioned above by plotting not only the intensity, Figure 4a, but also the phase, Figure 4b, of the reflectance spectra: strong phase shifts are observed at positive angles of incidence as an indication of a resonance excitation, whereas no significant structure appears at negative angles of incidence. To confirm such excitation, a near-field pattern is shown in Figure 4c within a unit cell at a fixed height ($z = 100$ nm), upon illuminating the metasurface at the Brewster quasi-BIC wavelength ($\lambda \sim 532$ nm) and angle of incidence $\theta = +5°$: a vertical magnetic field pattern with a large intensity (normalized to that of the incident field) and the expected spatial distribution confirms the coupling into the MD-induced Brewster quasi-BIC. If the angular/spectral dependence of the intensity of such component at the unit cell center is plotted, see Figure 4d, as in Figure 4a and b, the asymmetry in the coupling into the Brewster quasi-BIC is clearly manifested. Finally, we make sure of such asymmetry by showing the vertical near-field magnetic field intensity spectra along one unit-cell direction at a fixed angle of incidence at $\theta = \pm 5°$ in Figure 4e and f: if the direction of the incoming field is the mirror-symmetric of that of the MO-induced tilting of the vertical MD resonance (with respect to the plane normal to both the metasurface and the plane of incidence, see schematic in Figure 4g), a strong near-field enhancement is observed in the center of the unit cell; by contrast, if the direction of the incoming field is that of the MO-induced tilting of the vertical MD resonance (see schematic in Figure 4h), the near-field spectra show no significant enhancement. Recall the equivalence between $\pm\theta$ angles of incidence and reversing the applied magnetic field direction.

Thereby, we unveil a mechanism to magneto-optically induced switching on/off of an MO (equivalent to Brewster) quasi-BIC with a large Q-factor by simply reversing the magnetic field direction as in Figure 4g and h. The advantage with respect to conventional quasi-BICs is their "transparent" behavior, leaving unaltered the incoming beam, while switching on/off the excitation within the metasurface of the MD-related MO-quasi-BIC, which can be in turn exploited to enhance nonlinear processes, lasing, or sensing. Incidentally, it should be emphasized that the presence of a dielectric substrate has no significant impact on the above-mentioned phenomenology. In practice, index-matching layers can be used to cover the sample so that the environment is homogeneous as in Ref. [9], an approach which even allowed for BIC-induced lasing [12]; moreover, if an index jump still exists, as long as the resonant dipolar behavior is preserved, BICs emerge with the only impact of a slightly (substrate-induced) shift of the resonance frequency [8].

5 Bi:YIG nanodisk metasurface

We now extend the MO-BIC analysis to a more practical configuration. With the aim of decoupling the BIC from the broad resonance backgrounds, disk shapes are considered. The chosen MO active material is Bismuth substituted

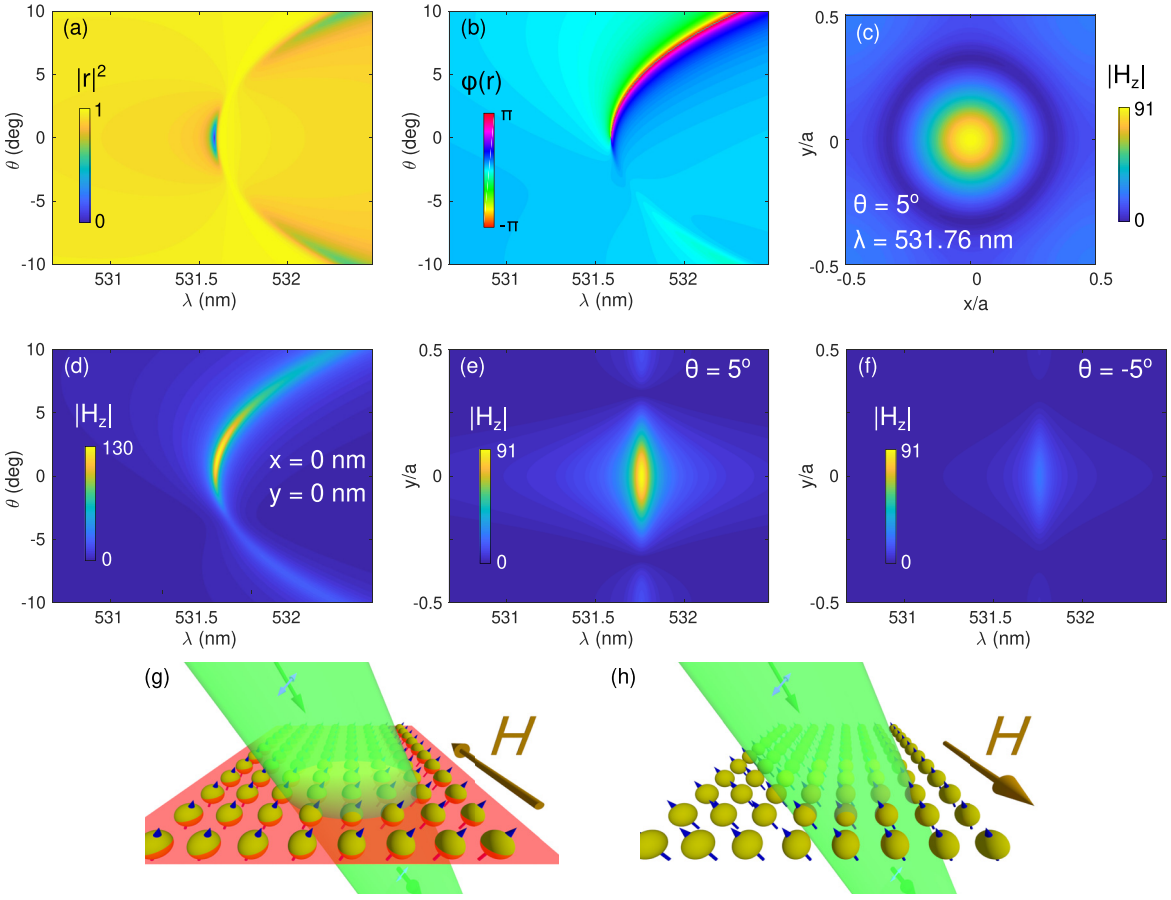

Figure 4: (a and b) Contour maps of the (a) intensity and (b) phase of the reflectance complex amplitude $r(\omega)$ (where $R(\omega) = |r(\omega)|^2$) for TE polarization from an infinite square array of lossless semiconductor ($n = 3.5$) nanospheres (lattice period $a = 300$ nm, sphere diameter $D = 150$ nm), as in Figure 2a and c, but for fixed MO activity $\beta = 1$, as a function of the angle of incidence and wavelength λ, theoretically calculated through CEMD, exploring the angular dependence of the MD quasi-BIC. (c–f) Contour maps of the amplitude of the vertical magnetic near-field, calculated also through our analytical CEMD theory, all of them at a distance of $z = 100$ nm above the square array: (c) within a unit cell at the wavelength ($\lambda = 531.76$ nm) and angle $\theta = 5°$ of the Brewster quasi MO-BIC; (d) spectral and angular dependence as in (a and b); (e and f) spectral dependence of cuts along one of the in-plane axes within the unit cell, at two fixed angles of incidence (e) $\theta = 5°$ and (f) $\theta = -5°$ (equivalent to two antiparallel magnetic field directions at a fixed angle of incidence). (g and h) Illustration of the switching concept based on reversing the direction of the magnetic field at a fixed angle of incidence, (g) with and (h) without coupling into the Brewster quasi-BIC, equivalent to the configurations based on symmetric angles of incidence and fixed magnetic field shown, respectively, in (e) and (f).

Yttrium Iron Garnet (Bi:YIG). Apart from being a dielectric medium with a relatively large, almost lossless dielectric constant in the visible domain (nearly dispersionless in the 500–600 nm range, $\epsilon_{\text{Bi:YIG}} \sim 5.5$) [47, 48], Bi:YIG disks are in turn amenable to nanofabrication.

We calculate through FDTD numerical simulations (as detailed above) the reflectance spectrum at normal incidence (TE polarization) and fixed MO activity: the latter is assumed saturated and leading to a nondiagonal permittivity $\epsilon_{xz}^{(\text{MO})} = -\epsilon_{zx}^{(\text{MO})} = 0.01\imath$, with a configuration identical to the schematic in Figure 1a. The result is shown in Figure 5. The main advantage of the disk shape as compared to the isotropic spheres is the fact that the vertical MD & ED resonances are decoupled from the in-plane resonances. Indeed, only the broad resonance due to the in-plane MDs is observed in Figure 5 at $\lambda = 505$ nm. The MO impact on the canonical BIC is revealed as a narrow peak at $\lambda \sim 583$ nm over a weak background. Its extremely narrow width (high Q-factor) and asymmetric (Fano) line shape are evidenced in the inset, demonstrating the BIC detuning at the Γ point controlled by the applied magnetic field, converting it into a quasi-BIC accessible through plane wave illumination. This confirms that Bi:YIG disk metasurfaces could also be utilized for MO (active) tuning and switching of Brewster quasi BICs. It is worth noting that we have discarded the small losses in

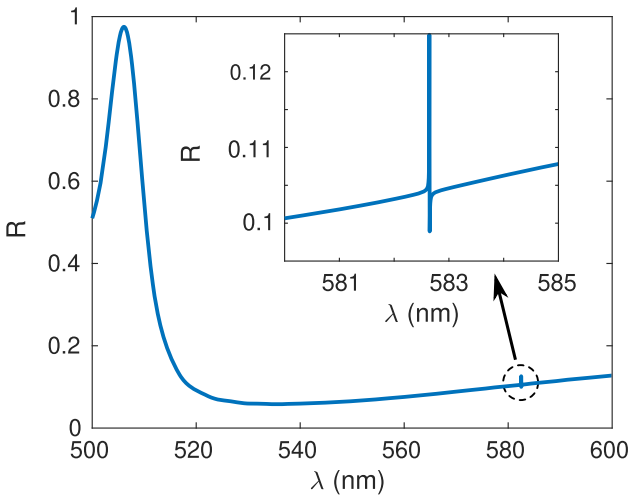

Figure 5: Reflectance spectra $R(\omega)$ from an infinite square array (lattice period $a = 340$ nm) of Bi:YIG ($\epsilon_{\text{Bi:YIG}} \sim 5.5$) nanodisks (150 nm radius and 120 nm height), for fixed MO activity (see text), calculated through FDTD simulations for TE polarization.

both the diagonal ($\epsilon_{\text{Bi:YIG}} \sim 5.5 + 0.0025\imath$) and off-diagonal ($\epsilon_{xz}^{(\text{MO})} \sim \imath(0.01 - 0.0015\imath)$) permittivity terms, since they have no impact on the phenomenology other than providing upper limits to the quasi-BIC Q-factors, as shown in Refs. [8, 9].

6 Concluding remarks

In summary, we have shown how to actively tune a canonical BIC in all-dielectric metasurfaces through MO activity. As a proof of principle, a square array of lossless semiconductor spheres is first considered, revealing through our CEMD model and FDTD simulations how the MO activity turns the BIC into a quasi-BIC with an extremely large, but finite Q-factor. In addition, this MO-tuned BIC is shown to be analytically equivalent to tilting the vertical-dipole resonance responsible for the BIC emergence, much in the same way as Brewster quasi-BICs [7]. Such resemblance is exploited to turn BICs into quasi-BICs by increasing the magnetic field applied parallel to the planar array, thus making Brewster quasi-BICs emerge at desired (MO-tuned) angles of incidence. In addition, we propose a switching mechanism by simply reversing the magnetic field direction, allowing to choose whether or not the high-Q MO (Brewster) quasi-BIC is excited (on/off state) with strong resonant-like near-field patterns. The active MO control of a Brewster quasi-BIC in the optical domain is further confirmed in a realistic Bi:YIG nanodisk metasurface through numerical simulations. Our results reveal a simple mechanism to actively (and fastly) tune/switch quasi BICs with obvious applications in sensing, filtering, slow light, and nonlinear optics.

Author contribution: All the authors have accepted responsibility for the entire content of this submitted manuscript and approved submission.
Research funding: Financial support is acknowledged from the Spanish Ministerio de Ciencia e Innovación (MICIU/AEI/FEDER,UE) through the grants PGC2018-095777-B-C21 (MELODIA) and PID2019-109905GA-C22, and from the Ministerio de Educación, Cultura y Deporte through a PhD Fellowship (FPU15/03566). J.-M. Llorens acknowledges funding from MINECO RYC-2017-21995, PID2019-106088RB-C31 and support from CSIC Research Platform PTI-001.
Conflict of interest statement: The authors declare no conflicts of interest regarding this article.

References

[1] C. W. Hsu, B. Zhen, A. D. Stone, J. D. Joannopoulos, and M. Soljačić, "Bound states in the continuum," *Nat. Rev. Mater.*, vol. 1, no. 9, p. 16048, 2016.
[2] D. C. Marinica, A. G. Borisov, and S. V. Shabanov, "Bound states in the continuum in photonics," *Phys. Rev. Lett.*, vol. 100, no. 18, p. 183902, 2008.
[3] C. W. Hsu, B. Zhen, J. Lee, et al., "Observation of trapped light within the radiation continuum," *Nature*, vol. 499, no. 7457, pp. 188–191, 2013.
[4] E. N. Bulgakov and A. F. Sadreev, "Bloch bound states in the radiation continuum in a periodic array of dielectric rods," *Phys. Rev. A*, vol. 90, no. 5, p. 53801, 2014.
[5] K. Koshelev, A. A. Bogdanov, and Y. Kivshar, "Meta-optics and bound states in the continuum," *Sci. Bull.*, vol. 64, no. 12, pp. 836–842, 2019.
[6] K. Koshelev, S. Lepeshov, M. Liu, A. A. Bogdanov, and Y. Kivshar, "Asymmetric metasurfaces with high-Q resonances governed by bound states in the continuum," *Phys. Rev. Lett.*, vol. 121, no. 19, p. 193903, 2018.
[7] D. R. Abujetas, Á. Barreda, F. Moreno, et al., "Brewster quasi bound states in the continuum in all-dielectric metasurfaces from single magnetic-dipole resonance meta-atoms," *Sci. Rep.*, vol. 9, no. 1, p. 16048, 2019.
[8] D. R. Abujetas, N. van Hoof, S. T. Huurne, J. G. Rivas, and J. A. Sánchez-Gil, "Spectral and temporal evidence of robust photonic bound states in the continuum on terahertz metasurfaces," *Optica*, vol. 6, no. 8, p. 996, 2019.
[9] S. Murai, D. R. Abujetas, G. W. Castellanos, J. A. Sánchez-Gil, F. Zhang, and J. G. Rivas, "Bound states in the continuum in the visible emerging from out-of-plane magnetic dipoles," *ACS Photonics*, vol. 7, no. 8, pp. 2204–2210, 2020.
[10] A. Kodigala, T. Lepetit, Q. Gu, B. Bahari, Y. Fainman, and B. Kanté, "Lasing action from photonic bound states in continuum," *Nature*, vol. 541, no. 7636, pp. 196–199, 2017.

[11] S. T. Ha, Y. H. Fu, N. Kumar Emani, et al., "Directional lasing in resonant semiconductor nanoantenna arrays," *Nat. Nanotechnol.*, vol. 13, no. 11, pp. 1042–1047, 2018.
[12] M. Wu, S. T. Ha, S. Shendre, et al., "Room-temperature lasing in colloidal nanoplatelets via mie-resonant bound states in the continuum," *Nano Lett.*, vol. 20, no. 8, pp. 6005–6011, 2020.
[13] L. Carletti, K. Koshelev, C. De Angelis, and Y. Kivshar, "Giant nonlinear response at the nanoscale driven by bound states in the continuum," *Phys. Rev. Lett.*, vol. 121, no. 3, p. 033903, 2018.
[14] Z. Han, F. Ding, Y. Cai, and U. Levy, "Significantly enhanced second-harmonic generations with all-dielectric antenna array working in the quasi-bound states in the continuum and excited by linearly polarized plane waves," *Nanophotonics*, vol. 10, no. 3, pp. 1189–1196, 2021.
[15] D. R. Abujetas, Á. Barreda, F. Moreno, A. Litman, J.-M. Geffrin, and J. A. Sánchez-Gil, "High-Q transparency band in all-dielectric metasurfaces induced by a quasi bound state in the continuum," *Laser Photon. Rev.*, vol. 15, no. 1, p. 2000263, 2021.
[16] F. Yesilkoy, E. R. Arvelo, Y. Jahani, et al., "Ultrasensitive hyperspectral imaging and biodetection enabled by dielectric metasurfaces," *Nat. Photonics*, vol. 13, no. 6, pp. 390–396, 2019.
[17] D. R. Abujetas, J. J. Sáenz, and J. A. Sánchez-Gil, "Narrow Fano resonances in Si nanocylinder metasurfaces: refractive index sensing," *J. Appl. Phys.*, vol. 125, no. 18, p. 183103, 2019.
[18] Y. Che, X. Wang, Q. Song, Y. Zhu, and S. Xiao, "Tunable optical metasurfaces enabled by multiple modulation mechanisms," *Nanophotonics*, vol. 9, no. 15, pp. 4407–4431, 2020.
[19] B. Yu, L. Huang, X. Li, and Y. Wang, "Magnetically controllable metasurface and its application," *Front. Optoelectron.*, vol. 4, no. 2, pp. 154–169, 2021.
[20] K. Fan, I. V. Shadrivov, and W. J. Padilla, "Dynamic bound states in the continuum," *Optica*, vol. 6, no. 2, p. 169, 2019.
[21] S. Han, L. Cong, Y. K. Srivastava, et al., "All-dielectric active terahertz photonics driven by bound states in the continuum," *Adv. Mater.*, vol. 31, no. 37, p. 1901921, 2019.
[22] M. Mahdi Salary and H. Mosallaei, "Tunable all-dielectric metasurfaces for phase-only modulation of transmitted light based on quasi-bound states in the continuum," *ACS Photonics*, vol. 7, no. 7, pp. 1813–1829, 2020.
[23] E. Mikheeva, K. Koshelev, D.-Y. Choi, et al., "Photosensitive chalcogenide metasurfaces supporting bound states in the continuum," *Opt. Express*, vol. 27, no. 23, p. 33847, 2019.
[24] G. Y. Chen, W. X. Zhang, and X. D. Zhang, "Strong terahertz magneto-optical phenomena based on quasi-bound states in the continuum and Fano resonances," *Opt. Express*, vol. 27, no. 12, p. 16449, 2019.
[25] X. Chen and W. Fan, "Tunable bound states in the continuum in all-dielectric terahertz metasurfaces," *Nanomaterials*, vol. 10, no. 4, p. 623, 2020.
[26] C. B. Rojas Hurtado, J. Dickmann, F. F. Bruns, T. Siefke, and S. Kroker, "Bound states in the continuum for optomechanical light control with dielectric metasurfaces," *Opt. Express*, vol. 28, no. 14, p. 20106, 2020.
[27] B. R. Wu, J. H. Yang, P. S. Pankin, et al., "Quasi-bound states in the continuum with temperature-tunable Q factors and critical coupling point at brewster's angle," *Laser Photon. Rev.*, vols 1–7, p. 2000290, 2021.
[28] S. I. Azzam and A. V. Kildishev, "Photonic bound states in the continuum: from basics to applications," *Adv. Opt. Mater.*, vol. 9, no. 1, p. 2001469, 2021.
[29] A. M. Chernyak, M. G. Barsukova, A. S. Shorokhov, A. I. Musorin, and A. A. Fedyanin, "Bound states in the continuum in magnetophotonic metasurfaces," *JETP Lett.*, vol. 111, no. 1, pp. 46–49, 2020.
[30] D. O. Ignatyeva, D. Karki, A. A. Voronov, et al., "All-dielectric magnetic metasurface for advanced light control in dual polarizations combined with high-Q resonances," *Nat. Commun.*, vol. 11, no. 1, p. 5487, 2020.
[31] V. V. Temnov, G. Armelles, U. Woggon, et al., "Active magneto-plasmonics in hybrid metal–ferromagnet structures," *Nat. Photonics*, vol. 4, no. 2, pp. 107–111, 2010.
[32] G. Armelles, A. Cebollada, A. García-Martín, and M. U. González, "Magnetoplasmonics: combining magnetic and plasmonic functionalities," *Adv. Opt. Mater.*, vol. 1, no. 1, pp. 10–35, 2013.
[33] J. F. Torrado, J. B. González-Díaz, A. García-Martín, and G. Armelles, "Unraveling the relationship between electromagnetic field intensity and the magnetic modulation of the wave vector of coupled surface plasmon polaritons," *New J. Phys.*, vol. 15, no. 7, p. 075025, 2013.
[34] N. Maccaferri, I. Zubritskaya, I. Razdolski, et al., "Nanoscale magnetophotonics," *J. Appl. Phys.*, vol. 127, no. 8, p. 080903, 2020.
[35] R. M. Rowan-Robinson, J. Hurst, A. Ciuciulkaite, et al., "Direction-sensitive magnetophotonic surface crystals," *Adv. Photon. Res.*, p. 2100119, 2021 [Online]. Available at: https://doi.org/10.1002/adpr.202100119.
[36] M. G. Manera, A. Colombelli, A. Taurino, A. Garcia Martin, and R. Rella, "Magneto-Optical properties of noble-metal nanostructures: functional nanomaterials for bio sensing," *Sci. Rep.*, vol. 8, no. 1, p. 12640, 2018.
[37] N. Maccaferri, K. E. Gregorczyk, T. V. A. G. de Oliveira, et al., "Ultrasensitive and label-free molecular-level detection enabled by light phase control in magnetoplasmonic nanoantennas," *Nat. Commun.*, vol. 6, no. 1, p. 6150, 2015.
[38] B. Caballero, A. García-Martín, and J. C. Cuevas, "Hybrid magnetoplasmonic crystals boost the performance of nanohole arrays as plasmonic sensors," *ACS Photonics*, vol. 3, no. 2, pp. 203–208, 2016.
[39] R. M. A. Ekeroth, P. Ben-Abdallah, J. C. Cuevas, and A. García-Martín, "Anisotropic thermal magnetoresistance for an active control of radiative heat transfer," *ACS Photonics*, vol. 5, no. 3, pp. 705–710, 2018.
[40] J. Song, Q. Cheng, L. Lu, et al., "Magnetically tunable near-field radiative heat transfer in hyperbolic metamaterials," *Phys. Rev. Appl.*, vol. 13, p. 024054, 2020.
[41] D. R. Abujetas, J. Olmos-Trigo, J. J. Sáenz, and J. A. Sánchez-Gil, "Coupled electric and magnetic dipole formulation for planar arrays of particles: resonances and bound states in the continuum for all-dielectric metasurfaces," *Phys. Rev. B*, vol. 102, no. 12, p. 125411, 2020.

[42] D. R. Abujetas and J. A. Sánchez-Gil, "Near-field excitation of bound states in the continuum in all-dielectric metasurfaces through a coupled electric/magnetic dipole model," *Nanomaterials*, vol. 11, no. 4, p. 998, 2021.
[43] N. de Sousa, L. S. Froufe-Pérez, J. J. Sáenz, and A. García-Martín, "Magneto-optical activity in high index dielectric nanoantennas," *Sci. Rep.*, vol. 6, no. 1, p. 30803, 2016.
[44] S. Dey and R. Mittra, "Efficient computation of resonant frequencies and quality factors of cavities via a combination of the finite-difference time-domain technique and the pade approximation," *IEEE Microw. Guid. Wave Lett.*, vol. 8, no. 12, pp. 415–417, 1998.
[45] I. Prieto, J. Herranz, L. Wewior, et al., "High quality factor gas-based photonic crystal microcavities by epitaxial re-growth," *Opt. Express*, vol. 21, no. 25, pp. 31615–31622, 2013.
[46] A. Bruner, D. LaMaster, and K. Lopata, "Accelerated broadband spectra using transition dipole decomposition and padé approximants," *J. Chem. Theor. Comput.*, vol. 12, no. 8, pp. 3741–3750, 2016, PMID: 27359347.
[47] S. Wittekoek, T. J. A. Poprna, J. M. Robertson, and P. F. Bongers, "Magneto-optic spectra and the dielectric tensor elements of bismuth-substituted iron garnets at photon energies between 2.2–5.2 ev," *Phys. Rev. B*, vol. 12, pp. 2777–2788, 1975.
[48] V. I. Belotelov, L. L. Doskolovich, V. A. Kotov, E. A. Bezus, D. A. Bykov, and A. K. Zvezdin, "Magnetooptical effects in the metal-dielectric gratings," *Opt. Commun.*, vol. 278, pp. 104–109, 2007.